Evaluation of Direct Inversion of Proton Radiographs in the Context of Cylindrical Implosions

J. R. Davies and P. V. Heuer

Laboratory for Laser Energetics, University of Rochester

Proton radiography is frequently used on OMEGA and OMEGA EP to infer electric and magnetic fields. If proton energy loss and scattering are negligible, proton deflection at the detector will be determined by the path-integrated transverse Lorentz force experienced by the protons. The most common technique used to infer fields from intensity modulations on the detector has been proton tracing in given fields, either assumed or obtained from simulations. Recently, a number of authors have used direct inversion to infer the fields,[1–6] and many of these direct inversion routines are publicly available on GitHub.[1–5] Direct inversion provides a solution independent of biases; particle tracing in specified forces is subject to user biases, and tracing in forces determined from simulations is limited by knowledge of the experimental conditions to be simulated and the physics included in the simulations. Publicly available direct inversion routines were applied to proton radiography data from cylindrical implosion experiments on OMEGA. As a first step, a series of test problems is generated using proton tracing to evaluate the routines.[7] These test problems are publicly available[8] as hdf5 files in pradformat.[9] The test results are summarized here.

Direct inversion determines deflections at the detector that map the source intensity (I_0) to the measured intensity (I). There is no unique solution to this problem, as demonstrated by the trivial case of simply swapping two particles on the detector. There is a unique solution, however, that minimizes total deflection and does not allow particles to be moved over one another. If proton trajectories to the detector do not cross, direct inversion will give the solution. If proton trajectories do cross, direct inversion will give one out of an infinite family of solutions, which is still useful information. In mathematics, direct inversion is known as the optimal transport problem, first described in a paper by Monge published in 1781 (Ref. 10), which derives what is now known as the Monge–Ampère equation. All but one of the publicly available direct inversion routines solve the Monge–Ampère equation.[1–4] The other routine[5] uses iterative methods to construct power diagrams (weighted Voronoi diagrams) of the source and measured intensities with equal flux in each cell, determining the deflections from the movement of cell centroids. Direct inversion can be applied to radiography with any charged particle, and to shadowgraphy where photons are deflected by gradients in refractive index.[5] In order to relate the deflections obtained at the detector to the forces in the object, one must assume a small angle deflection in the object ($\ll$1 rad or 57.3°) so that the deflections are proportional to the line-integrated force along the original trajectory. In practice, this is not a major restriction since the proton radiography and shadowgraphy setups used on OMEGA and OMEGA EP subtend a small angle at the target. If there are regions where large angle deflections occur, information on the forces in these regions will be lost.

Test radiographs or, equivalently, shadowgraphs, were generated by particle tracing through purely radial force profiles in cylinders and spheres for a range of force amplitudes with uniform source intensities. In cylinders a Gaussian potential [$F_r \propto r \exp(-r^2/R_2)$], a linear profile ($F_r \propto r$ for $r \leq R$)], and a top-hat profile (F_r = constant for $r \leq R$) were used. The linear profile was chosen to represent the electric field in an isothermal, cylindrical expansion,[11] ignoring the rapidly decaying field in the electron sheath beyond the ion front. The top-hat profile was chosen to represent the axial magnetic field in a cylindrical implosion, which is discontinuous at the inner surface of the shell. For spheres, a Gaussian potential was used. Force is expressed as a dimensionless parameter

$$\mu = \frac{2LF}{Mpv},$$

where L is object-to-detector distance, M is magnification, F is Lorentz force, p is particle momentum, and v is particle velocity, or

$$\mu = \frac{L}{\mathrm{M}} \frac{\mathrm{d}\left(n_\mathrm{e}/n_\mathrm{c}\right)/\mathrm{d}r}{\sqrt{1-n_\mathrm{e}/n_\mathrm{c}}}$$

for shadowgraphy, where n_e is electron density and n_c is the critical density of the probe. All distances are expressed in terms of the object size R. Trajectories cross in all cases for the linear and top-hat profiles and for both cylindrical and spherical Gaussian potentials when $\mu_{\max} \geq 1.08$ or $\mu_{\max} \leq -0.484$, negative values indicating a focusing force.

Five direct inversion routines were found on GitHub.[1–5] Two of the routines, both Monge–Ampère solvers, did not run.[1,2] The other two Monge–Ampère solvers were found to be essentially identical, which is not surprising considering they are implementations of the same algorithm by the same author.[3,4] Therefore, one Monge-Ampère routine and one power-diagram routine[5] was available to evaluate. The Monge–Ampère routine could not solve the cylindrical problems because it uses fixed deflection potential boundary conditions, which would also cause issues with any problem that has modulations near the boundary. The correct boundary conditions to obtain a minimum deflection from the Monge–Ampère equation are to set the deflections across the boundaries to zero.[2] The Monge-Ampère routine accurately inverted the spherical Gaussian tests when trajectories did not cross and did so roughly 1000× faster than the power-diagram routine, but failed when trajectories crossed. The failure was obvious from the poor reproduction of the measured intensity. The failure appears to be caused by the adaptive time step, which rapidly falls to the specified minimum value for tests where deflected trajectories cross. The power-diagram routine successfully inverted all but two of the test problems. The power diagram failed for the top-hat profile with $\mu_{\max} = 2$ and a smaller bin width (0.015R) than the final value we settled on (0.025R); however, for the coarser bin width an adequate solution was obtained. The power-diagram routine failed for a spherical Gaussian with $\mu_{\max} = -0.5$ and the issue was not resolved by coarser binning, the bin width of 0.052R already being too coarse to resolve the sharp peak. The power-diagram routine moves the sites closest to the corners into the corners in order to interpolate the deflections to all points on the original grid, which, for this strongly focusing test, leads to significant distortion of the entire region. Examples of the line-integrated forces obtained by the power-diagram routine for the cylindrical tests are given in Fig. 1. In all cases the measured intensity was accurately reproduced. The inversion underestimates the original line-integrated forces when trajectories cross because it gives a minimum deflection solution. It should be remembered that when trajectories cross, there exists an infinite family of solutions for the line-integrated force. As a result of these tests, only the power-diagram routine was used to analyze the proton radiographs of cylindrical implosions.[12]

This material is based upon work supported by the U. S. Department of Energy's Advanced Research Projects Agency-Energy under Award Number DE-AR0000568 and National Nuclear Security Administration under Award Number DE-NA0003856, the University of Rochester, and the New York State Energy Research and Development Authority.

1. C. Graziani *et al.*, Rev. Sci. Instrum. **88**, 123507 (2017).
2. A. F. A. Bott *et al.*, J. Plasma Phys. **83**, 905830614 (2017); PROBLEM Solver (PROton-imaged B-field nonLinear Extraction Module), Accessed 12 July 2021, https://github.com/flash-center/PROBLEM.
3. M. F. Kasim, Invert Shadowgraphy and Proton Radiography, Accessed 8 July 2021, https://github.com/mfkasim1/invert-shadowgraphy.
4. M. F. Kasim *et al.*, Phys. Rev. E **100**, 033208 (2019); M. F. Kasim, PRNS (Proton Radiography with No Source), Accessed 12 July 2021, https://github.com/OxfordHED/proton-radiography-no-source.
5. M. F. Kasim *et al.*, Phys. Rev. E **95**, 023306 (2017); M. F. Kasim, Invert Shadowgraphy and Proton Radiography, Accessed 8 July 2021, https://github.com/mfkasim1/invert-shadowgraphy.
6. N. F. Y. Chen *et al.*, Phys. Rev. E **95**, 043305 (2017).
7. J. R. Davies and P. V. Heuer, "Evaluation of Direct Inversion of Proton Radiographs in the Context of Cylindrical Implosions," Physics Archive: https://doi.org/10.48550/arXiv.2203.00495 (2022).
8. J. Davies and P. Heuer, Synthetic Proton Radiographs for Testing Direct Inversion Algorithms, Zenodo, Accessed 3 August 2022, https://doi.org/10.5281/zenodo.6632986.

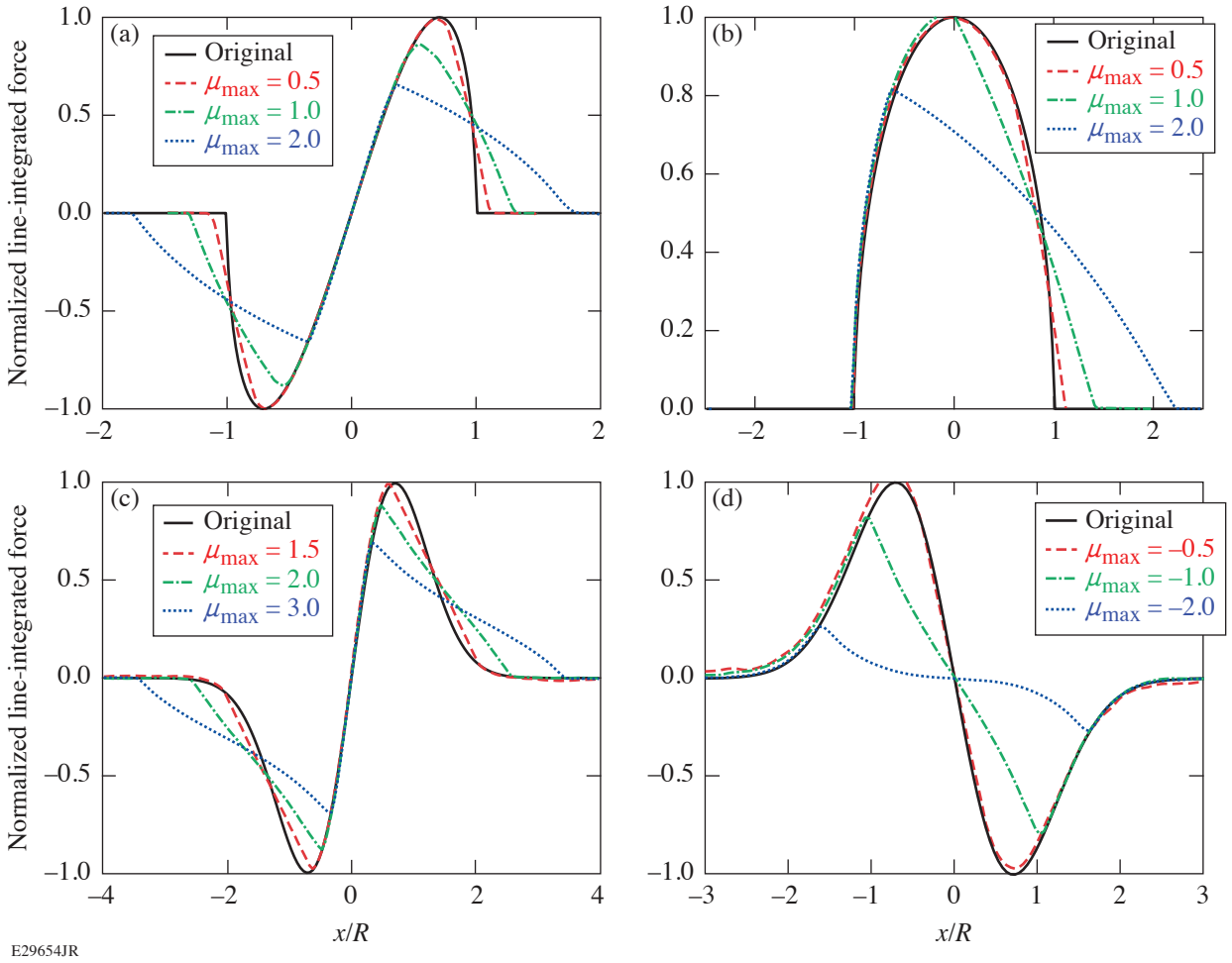

Figure 1
Line-integrated forces from the power-diagram routine for cylindrical test problems from (a) the linear profile, (b) the top-hat profile, and [(c),(d)] the Gaussian potential, normalized so that the maximum of the original is 1.

9. Pradformat (Proton Radiography File Format Tools), Accessed 12 July 2021, https://github.com/phyzicist/pradformat.
10. G. Monge, Mém. de l'Ac. R. des. Sc. An., 666 (1781).
11. M. Murakami and M. M. Basko, Phys. Plasmas **13**, 012105 (2006).
12. P. V. Heuer *et al.*, Phys. Plasmas **29**, 072708 (2022).